APS physics

CHORUS

This is the accepted manuscript made available via CHORUS. The article has been published as:

# Demonstration of enhanced broadband unidirectional electromagnetic radiation enabled by a subwavelength profile leaky anisotropic zero-index metamaterial coating

Zhi Hao Jiang, Qi Wu, and Douglas H. Werner

Phys. Rev. B **86**, 125131 — Published 21 September 2012

DOI: 10.1103/PhysRevB.86.125131

# Demonstration of Enhanced Broadband Unidirectional Electromagnetic Radiation Enabled by a Subwavelength Profile Leaky Anisotropic Zero-Index Metamaterial Coating

Zhi Hao Jiang, Qi Wu, and Douglas H. Werner
*Department of Electrical Engineering, The Pennsylvania State University,*
*University Park, PA 16802, USA*
*Corresponding Author Email: dhw@psu.edu*

In this paper, we report a technique for creating broadband unidirectional electromagnetic radiation with a grounded nonmagnetic anisotropic zero-index metamaterial coating. We demonstrate that the leaky modes supported by the finite sized coating structure can be exploited to create a unidirectional radiation device with a subwavelength thickness of only $0.12\lambda$. Numerical simulations and experimental characterization of the metamaterial-enabled radiator confirm the physical mechanisms governing its performance, showing a stable directive beam with an over 5-fold radiation power enhancement at broadside. Due to the resulting nonmagnetic material properties, this approach provides a new path to highly efficient, small footprint, low profile, and broadband directive radiation devices for microwave and potentially even optical wavelength applications.

By virtue of the unique properties that metamaterials (MMs) possess, in recent years, a wealth of previously unattainable physical phenomena and functional devices have been demonstrated throughout the electromagnetics spectrum[1,2]. In particular, it was immediately recognized by the electromagnetic/optics community that this new technology could be exploited for controlling the radiation properties of electromagnetic sources, especially for creating unidirectional wave radiation, which is highly desirable for various practical applications such as radio-frequency (RF) antennas and terahertz/optical sources. Previously, two MM based techniques have been utilized to achieve such physical behavior, including the Fabry-Perot (FP) cavity[3-6] and volumetric zero-index metamaterials (ZIMs)[7-10]. The conventional FP cavity formed with a ground plane requires a device thickness of half the operating wavelength. In order to reduce the profile, several advanced FP cavity antennas incorporating MM surfaces with customized reflection phases were demonstrated to possess a subwavelength device thickness[3-6]. However, most of these FP cavities exhibit an enhanced directivity only over a narrow bandwidth, which considerably limits their utility. The other MM approach is achieved by covering the electromagnetic source with volumetric ZIMs, as first proposed by Enoch *et al*[7]. The working principle is based on refraction as light passes from a low to high index medium. It has also been demonstrated that volumetric anisotropic ZIMs (AZIMs), with one of the permittivity and/or permeability tensor parameters approaching zero, can give rise to directive radiation[8-10]. Different from their isotropic counterparts, these AZIMs are capable of directing the propagation of electromagnetic waves not only at interfaces, but also inside the MM as enforced by the unique dispersion relations they possess. However, such ZIM or AZIM lenses are usually electrically large in all three dimensions, increasing the net size and weight of the device.

Recently, it has been proposed that thin grounded MM slabs with negative or zero index of refraction can give rise to novel electromagnetic responses, such as surface wave suppression[11] and frequency dependent directive radiation[12-14]. In particular, it has been shown theoretically that the directive radiation is caused by wave leakage from the MM slab, which facilitates formation of a conical and/or a pencil beam[12-14]. These structures are generally much longer than a wavelength and support leaky waves with phase velocities slightly higher than that in free-space. As a result, the beam maxima direction drifts away from the broadside and varies as a function of frequency, making them not suitable for broadband unidirectional radiation. In this paper, we investigate broadband unidirectional emission generated from a subwavelength-thick nonmagnetic grounded AZIM. First, a formulation is presented of the fast-wave leaky modes supported by the grounded AZIM, indicating the possibility of achieving quasi-infinite phase velocity within the structure. A MM realization is then proposed with the prescribed performance and validated through both near- and far-field distributions calculated from full-wave simulations of an infinite array. Finally, experiments were performed by constructing a properly designed AZIM coating of only $0.12\lambda$ thick for a practical slot antenna, showing a

stable directive beam with over 5-fold radiated power enhancement at broadside throughout the entire band of interest from 5.4 to 6.2 GHz.

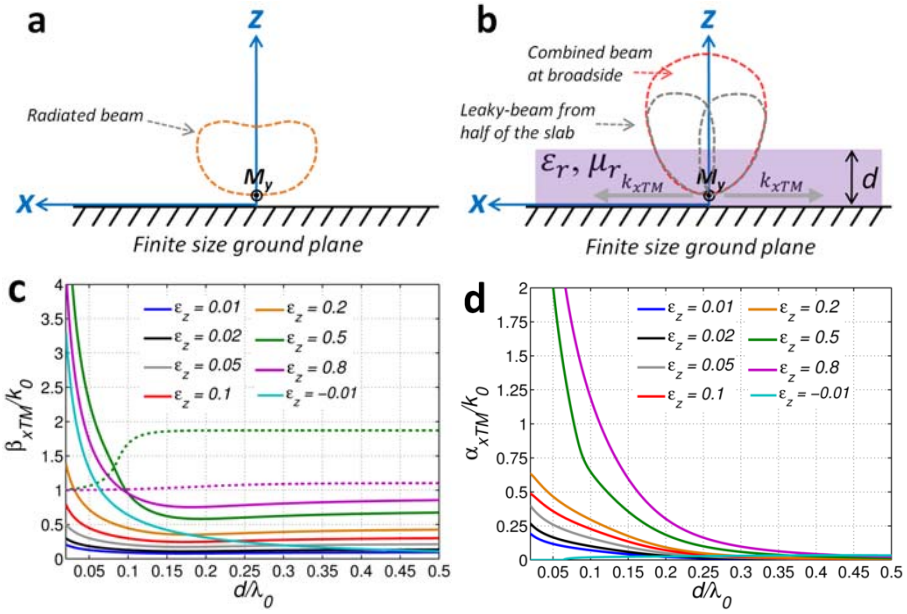


**FIG. 1** Unidirectional radiation pattern created by a magnetic current in conjunction with a low-profile grounded anisotropic coating. The size of the ground plane is comparable to a wavelength. (a) The radiated beam without the anisotropic coating has low directivity with its pattern affected by diffraction due to the finite ground plane. (b) With the anisotropic coating of thickness $d$, each half of the coating radiates a beam pointing close to broadside. The in-phase superposition of the two beams forms a unidirectional directive beam at broadside. (c) Real and (d) imaginary parts of the TM dispersion curves for a uniaxial anisotropic slab having $\varepsilon_t = 2.4$, and $\varepsilon_z = -0.01, 0.01, 0.02, 0.05, 0.1, 0.2, 0.5, 0.8$. The improper surface modes are indicated by dashed curves, while the leaky modes are represented by solid curves.

The configuration considered here consists of an anisotropic homogeneous slab, with a thickness of $d$, backed by a ground plane, as depicted in Fig.1. The slab is excited by a magnetic line source $\boldsymbol{M}$ located at $z = 0$ and oriented along the $y$ direction, resulting in transverse magnetic (TM) polarized waves ($H_y$, $E_x$, $E_z$) traveling in the $\pm x$ direction with a complex propagation constant, $k_{xTM} = \beta_{xTM} + i\alpha_{xTM}$. Such an arrangement can be regarded as two symmetric leaky slabs each radiating a single beam with the in-phase superposition of the two beams resulting in symmetrical radiation in the $x$-$z$ plane. The slab material is assumed to be linear and non-dispersive, with a uniaxial relative permittivity tensor represented by $\varepsilon_r = [\varepsilon_t, \varepsilon_t, \varepsilon_z]$ and a unity relative permeability $\mu_r = 1$. By assuming a harmonic time dependence as $\exp(-i\omega t)$ and no field variation in the $y$ direction ($k_y = 0$), the dispersion relations of TM polarized fields in free-space and inside the grounded anisotropic slab can be expressed as

$$k_{xTM}^2 + k_{0z}^2 = k_0^2 \text{ and } k_{xTM}^2/\varepsilon_z + k_z^2/\varepsilon_t = k_0^2 \tag{1}$$

respectively, where $k_0$ is the free-space wave number. The three field components in the anisotropic slab and free space regions can be written as

$$H_y^{as} = \frac{k_z A^{as}}{\mu_0 \mu_r}\cos(k_z z)e^{ik_{xTM}x}, \qquad H_y^{fs} = \frac{ik_{0z}A^{as}}{\mu_0}e^{ik_{0z}z}e^{ik_{xTM}x},$$

$$E_x^{as} = \frac{ik_z^2 A^{as}}{\omega\varepsilon_0\varepsilon_t\mu_0\mu_r}\sin(k_z z)e^{ik_{xTM}x}, \quad E_x^{fs} = \frac{ik_{0z}^2 A^{fs}}{\omega\varepsilon_0\mu_0}e^{ik_{0z}z}e^{ik_{xTM}x},$$

$$E_z^{as} = \frac{-k_x k_z A^{as}}{\omega\varepsilon_0\varepsilon_z\mu_0\mu_r}\cos(k_z z)e^{ik_{xTM}x}, \quad E_z^{fs} = \frac{-ik_x k_{0z} A^{fs}}{\omega\varepsilon_0\mu_0}e^{ik_{0z}z}e^{ik_{xTM}x}, \tag{2}$$

where the superscripts *as* and *fs* denote anisotropic slab and free space, respectively. The sine function is selected for $E_x^{as}$ due to the boundary condition at $z$=0 enforced by the presence of the ground plane. Based on the dispersion relations given in (1) and the field continuity conditions at the corresponding interfaces, the dispersion relation of the modes supported by the slab can be derived using the transverse resonance technique[15]. The resulting dispersion relation is given in (3) below:

$$\frac{\sqrt{k_0^2 - k_{xTM}^2}}{\omega} - i\frac{\sqrt{k_0^2\varepsilon_z - k_{xTM}^2}}{\omega\varepsilon_t}\sqrt{\frac{\varepsilon_t}{\varepsilon_z}}\tan\left(\sqrt{k_0^2\varepsilon_z - k_{xTM}^2}\sqrt{\frac{\varepsilon_t}{\varepsilon_z}}d\right) = 0 \tag{3}$$

It should be noted that the above equation is not only valid for slabs comprised of ordinary dielectric materials but also applicable to slabs with either zero or negative material tensor parameters[11]. This transcendental equation can be numerically solved to obtain the real and imaginary parts of $k_{xTM}$ as a function of frequency.

Fig. 1(c)-(d) presents the TM dispersion curves for a uniaxial anisotropic slab with a fixed $\varepsilon_t$ value of 2.4 and various $\varepsilon_z$ values. Several instructive characteristics can be identified. First, as $\varepsilon_z$ decreases the wave number of the improper surface modes drops and eventually the improper surface modes disappear, in which case the AZIM slab only supports unbounded leaky wave modes. Secondly, it can be observed that for all cases leaky modes with weak dispersion are supported in a broad frequency band. Finally, as $\varepsilon_z$ approaches zero from the right ($\varepsilon_z \to 0^+$), not only do the values of $\beta_{xTM}$ and $\alpha_{xTM}$ decrease, but their profiles also become flatter, indicating a more stable radiation beam direction near broadside across a wide frequency range. As a comparison, the dispersion curves for the anisotropic slab with $\varepsilon_z$ approaching zero from the left ($\varepsilon_z \to 0^-$) is also investigated. The dispersion relation for such a slab given in (1) becomes a hyperbolic function due to the negative sign of $\varepsilon_z$. As a result, the dispersion curve for $\varepsilon_z$ = -0.01 exhibits different behavior compared to its counterpart with $\varepsilon_z$ = 0.01. At high frequencies, where the electrical thickness of the slab is comparable to a half-wavelength, $\beta_{xTM}$ has a very small value, which is similar to the case where $\varepsilon_z$ = 0.01. As frequency decreases, the real part of $k_{xTM}$ monotonically grows, while the magnitude of its imaginary part first increases and then drops to zero where it remains. Physically, this indicates that the leaky wave mode supported by the slab transitions into an improper surface mode as the frequency decreases, which is not seen in the $\varepsilon_z$ = 0.01 case. This corroborates findings of previous work associated with isotropic slabs with near-zero, but negative permittivity values[15]. It should also be noted that, theoretically, when $\varepsilon_z$ exactly equals zero, $k_{xTM}$ is forced to be zero in order to satisfy the dispersion relation. As a result, the vanishing $z$ component of the electric displacement, *i.e.* $D_z$, in the slab forces $E_z$ to be zero in the free space region above the slab due to boundary condition, giving rise to the highest directivity achievable by such a grounded anisotropic slab. In order to achieve unidirectional radiation at broadside, the value of $\beta_{xTM}$ must be small according to the approximation that the radiated beam direction for each of the two anisotropic slabs (in -$x$ and +$x$) is given by $\theta_m = \sin^{-1}(\beta_{xTM}/k_0)$. If the anisotropic slab is electrically long, beam splitting will occur, as exhibited in conventional electrically long leaky wave antennas where directive broadside radiation is achieved at only one frequency[16]. Considering that the radiated beam width is proportional to $1/L_\lambda\cos(\theta_m)$, where $L_\lambda$ is the electrical length of the leaky slab, the two slightly squinted leaky beams with broader beam width can effectively superimpose and combine into one directive beam pointed at broadside. Hence, an AZIM slab with a finite lateral dimension comparable to the operational wavelength is preferred for generating unidirectional radiation. When a TM/quasi-TM source is properly excited at the bottom of the finite AZIM slab, a directive radiation device with a small footprint and subwavelength thickness can be achieved. Physically, the structure considered here operates differently from previously reported volumetric AZIM lenses, even though they share similar characteristics in their material parameters. For the volumetric AZIM, the field inside the lens is already well-collimated with no field tapering due to enforcement of the dispersion relation[9,10]. In contrast, field tapering is present within the grounded AZIM slab due to the complex propagation constant of the mode it supports.

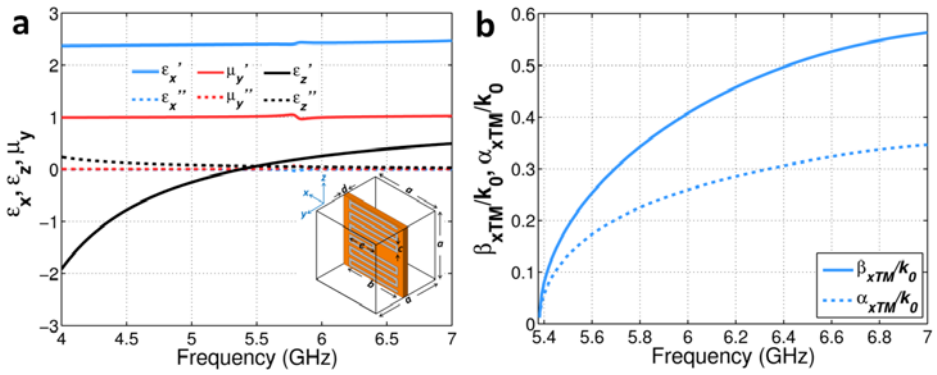


**FIG. 2** (a) Retrieved effective medium parameters ($\varepsilon_x$, $\varepsilon_z$, $\mu_y$) of the ELCWR array. The unit cell is shown in the inset. The dimensions are $a$ = 6.5, $b$ = 5.35, $c$ = 0.7, $d$ = 0.508, and $e$ = 2.8 (all in millimeters). The substrate material has a dielectric constant of 2.2. (b) The TM dispersion curves solved for using the retrieved effective medium parameters corresponding to a 6.5 mm thick grounded anisotropic slab.

To realize such an AZIM slab with subwavelength thickness, periodic end-loaded cut-wire resonators (ELCWR) were employed. The self-inductance of the wire and the capacitance between the end-load arms provide an electric dipole resonance. The unit cell geometry and dimensions are shown in the inset of Fig. 2(a). The retrieved effective medium parameters ($\varepsilon_x$, $\varepsilon_z$, $\mu_y$) for a doubly periodic ELCWR array, obtained from HFSS unit cell simulations together with an anisotropic parameter inversion algorithm[17], are shown in Fig. 2(a). The values of $\varepsilon_x$ and $\mu_y$ are virtually non-dispersive, while $\varepsilon_z$ exhibits a Lorentz-shaped electric resonance with an effective plasma frequency of 5.38 GHz. Furthermore, because the resonance tail is weakly dispersive, the value of $\varepsilon_z$ remains below 0.3 within the broad frequency range of 5.38 - 6.4 GHz. Simulations with multiple numbers of unit cells in the direction of wave propagation were also conducted, showing consistency in the retrieved effective medium parameter values (not shown here) compared to those obtained from a single layer structure, which corroborates results previously reported on weakly coupled metamaterial structures[18]. Moreover, the efficacy of using effective material parameters to describe electrically thin metamaterials, such as metafilms/metasurfaces, has been demonstrated through the design, analysis, and characterization of plasmonic quarter-wave plates and metamaterial-based gratings[19,20]. The transcendental equation for such a dispersive medium was then solved to obtain the TM dispersion curves shown in Fig. 2(b). It can be seen that at the effective plasma frequency, both $\beta_{xTM}$ and $\alpha_{xTM}$ are near zero, indicating a quasi-infinite phase velocity of the leaky wave. As frequency increases, both $\beta_{xTM}$ and $\alpha_{xTM}$ become larger due to the increasing value of $\varepsilon_z$. However, $\beta_{xTM}$ remains below $0.5k_x$ over a relatively broad bandwidth ranging from 5.38 to 6.4 GHz.

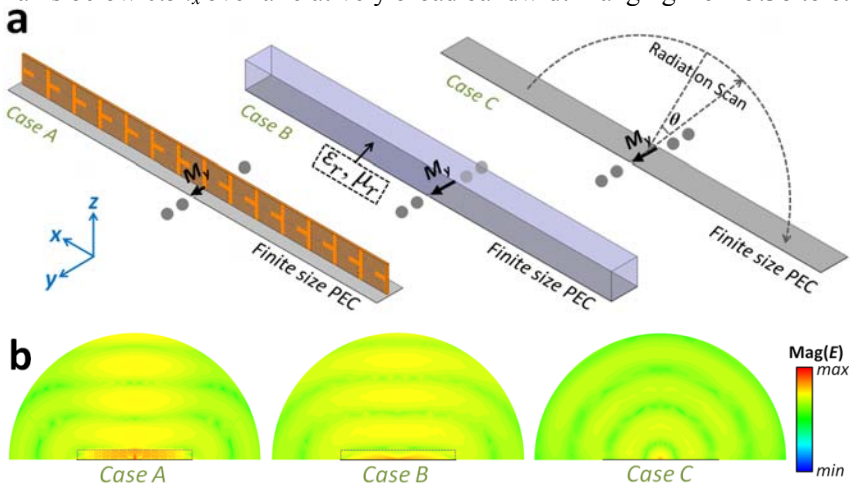

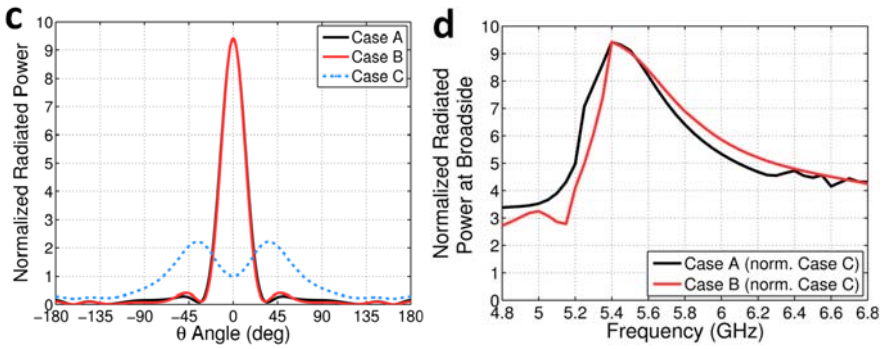


**FIG. 3** (a) Configuration of infinite array simulations for an actual AZIM coating, a dispersive effective medium slab, and the slot alone. The structures are infinite in the *y* direction with a periodicity of 6.5 mm. The finite sized PEC plane is 92 mm long in the *x* direction (underneath an AZIM coating with 14 cells). A perfectly matched absorbing slab is placed underneath the slots in the simulations to absorb the radiation in the *-z* half space. (b) Snapshots of *E*-field distributions in the upper *x*-*z* plane for the three cases. The blocks with dashed lines indicate the position of the MM coating or the effective medium slab. (c) Normalized radiated power for the three cases at 5.4 GHz (*i.e.* close to the effective plasma frequency of the MM). All the curves are normalized to Case C at broadside ($\theta = 0°$). (d) Normalized radiated power at broadside ($\theta = 0°$) as a function of frequency.

Full wave simulations were then carried out to investigate the radiation properties of the finite grounded AZIM coating using HFSS, a finite element solver. As illustrated in Fig. 3 (a), three cases were considered: (A) a 1mm wide slot covered by a single layer MM slab consisting of 14 cells in the *x* direction, (B) a 1mm wide slot covered by a dispersive effective medium (EM) slab with the retrieved $\varepsilon_r$ and $\mu_r$ tensors, and (C) a 1mm wide slot alone. The structures are infinitely long in the *y* direction with only the field components $H_y$, $E_x$, and $E_z$ existing in the far-zone, corresponding to the TM mode. The infinite slot, excited by an infinitesimal current source in the *x* direction, sufficiently approximates a TM line source. The far-field patterns (normalized to the value of Case C at broadside) in the upper *x*-*z* plane are presented in Fig. 3(c) for the three cases at 5.4 GHz. It can be observed that for the slot alone, the radiated wave is maximum close to $\theta = \pm 40°$ due to diffraction caused by the finite size of the ground plane in the *x* direction. However, with the actual MM or the EM slab the beam maximum is located at broadside and exhibits a significant 9-fold enhancement. The radiated beam is sharpened and the radiation in other directions is greatly suppressed compared to that generated by the slot alone. The enhancement of radiated power at broadside as a function of frequency is shown in Fig. 3(d). The maximum enhancement occurs at around 5.4 GHz, corresponding well to the effective plasma frequency predicted from the unit cell simulation. Within a broad frequency range from 5.2 - 6.4 GHz, the broadside radiation enhancement remains above 4.5-fold. The drop in the enhancement factor is caused by the dispersive nature of the leaky MM slab, as discussed previously. However, compared to conventional directive leaky-wave antennas, stable unidirectional radiation at broadside is achieved within a much broader bandwidth. The drop in the enhancement at frequencies below the peak is attributed to the fact that a partially negative anisotropic slab no longer supports a leaky mode with small tangential wave number. Overall, the numerical simulations show that the proposed subwavelength AZIM coating provides an efficient way of suppressing commonly encountered edge diffraction. In addition, the good agreement between the simulation results using the actual MM and the EM slab justifies the homogenization approximation employed here, which is assumed valid due to the subwavelength size of the unit cells.

The corresponding *E*-field distributions at 5.4 GHz (see Fig. 3(b)) in both the near- and far-field show well-collimated beams emanating from the slot covered with the actual MM or the EM slab. The symmetric field tapering along the *x* direction, observable in both the actual MM and the EM slab coatings, reveals the leaky nature of the structure. This also differentiates its physical operation from the volumetric AZIM lenses. Since 5.4 GHz is very close to the effective plasma frequency, the quasi-infinite phase velocity gives rise to a nearly ideal in-phase response over the entire aperture. Notably, the weak fields near the ends of the coating ensure the possibility of shrinking the footprint and lowering the profile of the device without sacrificing performance.

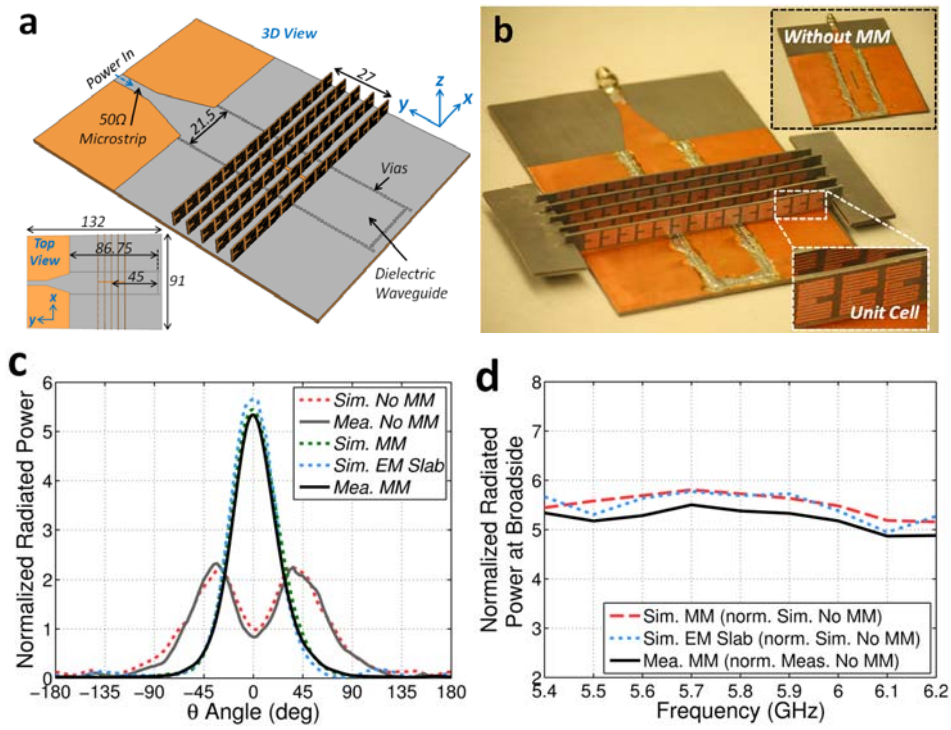


**FIG. 4** (a) Configuration of the AZIM coating on a half-wave slot antenna. The slot is etched on the top conducting surface of the dielectric waveguide and is fed by a microstrip. The size of the slot is 24.4 by 1.15 ($mm^2$). The dimensions labeled in the figure are all in millimeters. The substrate material for both the antenna and the MM coating is Rogers duroid/RT 5880 with $\varepsilon_r = 2.2 + 0.0198i$. (b) Photographs of the fabricated slot antenna and the MM coating. Additional dielectric slabs cut with interlocking slits were used on both sides of the AZIM coating to provide better mechanical support. The insets show the slot antenna alone and the magnified view of the MM unit cells. (c) Normalized radiated power at 5.4 GHz. All the curves are normalized to the predicted broadside ($\theta = 0°$) power of the slot antenna alone. (d) Normalized radiated power at broadside ($\theta = 0°$) as a function of frequency.

To experimentally demonstrate this AZIM coating, a practical slot antenna was utilized as a quasi-TM source. As Fig. 4(a) shows, for ease of feeding the input power, a microstrip fed substrate integrated dielectric waveguide (DW)[21] was employed with a half-wave slot cut out of it. Arrays of vias were used to effectively create electric walls, forming the DW with a $TE_{10}$ propagating mode. In order to obtain a good magnetic dipole mode on the slot, the distance between the center of the slot and the short-end of the waveguide was set to 3/4 of the slot resonant wavelength. Such a feeding structure possesses a much lower profile compared to a conventional rectangular waveguide. The dispersion of the DW limits the bandwidth of the magnetic dipole mode to within approximately 5.4 - 6.2 GHz. Instead of an infinite array in the $y$ direction as shown in Fig. 3(a), five rows of MM unit cells were cascaded in the $y$ direction to cover the half-wave slot. For comparison, a dispersive EM slab with the same size as the finite AZIM coating was also simulated. The combined AZIM coating and the DW fed slot antenna was fabricated, as shown in Fig. 4(b), with a net device thickness of only $0.12\lambda$ (at the center frequency). The far-field patterns of the radiated wave were measured in an anechoic chamber using a standard horn antenna. Since the $\varepsilon_x$ and $\mu_y$ of the AZIM coating have values close to those of free-space, the impedance of the slot antenna is not affected, *i.e.* the reflection at the power input port remains the same when covering the slot with the AZIM coating. The radiated power pattern at 5.4 GHz (normalized to the value of the simulated slot antenna alone at broadside) in the upper $x$-$z$ plane, are presented in Fig. 4(c). Excellent agreement can be observed between simulated and measured results, confirming a good realization of the designed AZIM. The simulation results using the EM slab also correspond well to those with the actual MM structure. Without the AZIM coating, a two-peak pattern is observed, due to the diffraction at the edge of the finite sized ground plane. In contrast, with the AZIM coating present, a distinct peak at broadside can be identified, with a 5.38-fold radiated power enhancement and suppressed radiation at angles away from broadside. The radiation power enhancement at broadside (normalized to the case of the slot alone) as a function of frequency is shown in Fig. 4(d). The measured results have slightly lower values (~ 0.3 - 0.4)

compared to simulations due to fabrication imperfections and additional losses introduced by the solder. Within the frequency range from 5.4 to 6.2 GHz where a magnetic dipole mode is properly excited, a radiated power enhancement of more than 5-fold is achieved. Different from the frequency response observed in Fig. 3(d) for an infinite array, the enhancement only varies slightly due to the frequency-dependent property of the actual antenna employed and the finite aperture of the MM coating. In practice, such stable enhancement is advantageous for various wireless systems due to its steady in-band frequency response. Considering that the footprint of the MM coating is only 91 by 32.5 $mm^2$, an aperture efficiency of over 90% is achieved throughout the band, indicating that the enhancement attained is approaching the theoretical limit.

When comparing to other types of devices for unidirectional radiation, such as the volumetric isotropic ZIM (IZIM), volumetric AZIM, Fabry-Perot cavity, and the conventional leaky wave antenna, the leaky AZIM approach presented in this work demonstrates unique properties and advantages as summarized in Table 1. First, the leaky AZIM and the volumetric AZIM can provide a broad operational bandwidth. On the contrary, the volumetric IZIM has a narrow bandwidth due to its stringent requirement of an isotropic zero/low index. Typical FP cavities have even narrower bandwidth due to the high Q factors of the associated cavity resonators. Conventional leaky wave antennas typically have a broad impedance bandwidth. However, their radiated beam steers as frequency the changes, leading to a very narrow broadside radiation bandwidth. Secondly, in terms of the profile of the device, conventional leaky wave antennas have extremely low profile due to their fully planar implementation. The leaky AZIM, as shown here, also possesses a very low profile, on the order of $\lambda/10$. The FP cavity has a typical thickness between a quarter and a half of the operating wavelength, although the thickness can be further reduced at the expense of severely sacrificed bandwidth. The volumetric IZIM and volumetric AZIM are both bulky in all three dimensions, especially in the direction of beam radiation, which is usually more than two wavelengths. Finally, in terms of the achievable directivity, the FP cavity provides the highest peak directivity due to the high Q resonance. Conventional leaky wave antennas can also provide a high directivity because of their electrically large lateral size, but the beam direction is not stable. Moreover, the proposed leaky AZIM device provides a higher directivity compared to the volumetric IZIM/AZIM[10]. In summary, the leaky AZIM approach demonstrated here provides an overall balanced performance by offering a low-profile, low-cost, compact footprint, and broadband directive unidirectional radiation.

Table 1. Property comparison among various unidirectional radiation techniques

| | **Leaky AZIM** | **Volumetric IZIM** | **Volumetric AZIM** | **FP Cavity** | **Conventional Leaky Antenna** |
|---|---|---|---|---|---|
| **Bandwidth** | Broad | Narrow | Broad | Very Narrow | Very Narrow (for broadside radiation) |
| **Profile** | Very Low | High | High | Low | Extremely Low |
| **Directivity** | High | Moderately High | Moderately High | Very High | High |

In conclusion, we have shown a new approach to achieve broadband unidirectional radiation using a thin grounded nonmagnetic AZIM coating. The complex leaky modes were studied and an actual MM design was proposed. Numerical simulations of an infinite array were carried out to validate the design, which also shed light on the underlying physical mechanisms governing the structure. This technique was further demonstrated by a prototype, producing a stable broadside directive radiation with more than a 5-fold enhancement in the frequency band of interest. Remarkably, even though this kind of AZIM coating possesses a small footprint and a subwavelength profile, it is nevertheless capable of providing broadband suppression of the commonly encountered edge diffraction effects which are associated with more conventional design approaches. These represent highly desirable properties for a variety of microwave applications. Furthermore, the nonmagnetic property of the MM coating makes it possible to realize these devices at terahertz frequencies and even optical wavelengths, which would broaden their applications to include enhanced optical transmission[22] and nanoantennas[23].

This work was supported by a NSF MRSEC under Grant DMR-0820404. The authors acknowledge fruitful discussions with D. Brocker, and thank S. Martin and P. Sieber for their assistance with the device fabrication.

[1] H. Chen, C. T. Chan, and P. Sheng, Nat. Mater. **9**, 387 (2010).
[2] N. Engheta and R. W. Ziolkowski, *Metamaterials: Physics and Engineering Explorations*. Wiley-IEEE Press 2006.
[3] A. P. Feresidis, G. Goussetis, S. Wang, and J. C. Vardaxoglou, IEEE Trans. Ant. Propagat. **53**, 209 (2005).
[4] L. Zhou, H. Li, Y. Qin, Z. Wei, and C. T. Chan, Appl. Phys. Lett. **86**, 101101 (2005).
[5] A. Ourir, A. Lustrac, and J.-M. Lourtioz, Appl. Phys. Lett. **88**, 084103 (2006).
[6] S. N. Burokur, J.-P. Daniel, P. Ratajczak, and A. Lustrac, Appl. Phys. Lett. **97**, 064101 (2010).
[7] S. Enoch, G. Tayeb, P. Sabouroux, N. Guerin, and P. Vincent, Phys. Rev. Lett. **89**, 213902 (2002).
[8] J. P. Turpin, A. T. Massoud, Z. H. Jiang, P. L. Werner, and D. H. Werner, Opt. Express **18**, 244 (2010).
[9] Q. Cheng, W. X. Jiang, and T. J. Cui, Appl. Phys. Lett. **99**, 131913 (2011).
[10] Z. H. Jiang, M. D. Gregory, and D. H. Werner, Phys. Rev. B **84**, 165111 (2011).
[11] P. Baccarelli, P. Burghignoli, G. Lovat, and S. Pailotto, IEEE Ant. Wireless Propagat. Lett. **2**, 269 (2003).
[12] G. Lovat, P. Burghignoli, F. Capolino, D. R. Jackson, and D. R. Wilton, IEEE Trans. Ant. Propagat. **54**, 1017 (2006).
[13] A. Alu, F. Bilotti, N. Engheta, and L. Vegni, IEEE Trans. Ant. Propagat. **55**, 882 (2007).
[14] A. Shahvarpour, C. Caloz, and A. Alvarez-Melcon, Radio Sci. **46**, RS4006, (2011).
[15] A. Alu, F. Bilotti, N. Engheta, and L. Vegni, IEEE Trans. Ant. Propagat. **55**, 1698 (2007).
[16] A. A. Oliner and D. R. Jackson, Antenna Engineering Handbook, 4th ed., Chapter 7, edited by J. L. Volakis, McGraw-Hill 2007.
[17] Z. H. Jiang, J. A. Bossard, X. Wang, and D. H. Werner, J. Appl. Phys. **109**, 101351 (2011).
[18] W.-C. Chen *et al.*, Phys. Rev. B **85**, 035112 (2012).
[19] B. Kanté, J.-M. Lourtioz, and A. de Lustrac, Phys. Rev. B **80**, 205120 (2009).
[20] Y. Zhao and A. Alù, Phys. Rev. B **84**, 205428 (2011).
[21] D. Deslandes and K. Wu, IEEE Trans. Microw. Theory Tech. **51**, 593 (2003).
[22] L. Martin-Moreno, F. J. Garcia-Vidal, H. J. Lezec, A. Degiron, and T. W. Ebbesen, Phys. Rev. Lett. **90**, 167401 (2003).
[23] L. Novotny and N. V. Hulst, Nat. Photon. **5**, 83 (2011).